


 Cite this: *RSC Adv.*, 2020, 10, 13083

Effective hydrogenation of carbonates to produce methanol over a ternary Cu/Zn/Al catalyst†

 Jiachen Li,^{abcd} Ligu Wang,^{id *abcdf} Xiang Hui,^{abcdg} Chanjuan Zhang,^{abcd} Yan Cao,^{ab} Shuang Xu,^{ab} Peng He^{ab} and Huiquan Li^{id *abcde}

Methanol synthesized from carbonate hydrogenation is of great importance for CO₂ utilization indirectly. Herein, a series of Cu/Zn/Al heterogeneous catalysts were prepared by co-precipitation with a synchronous aging step, and were applied for hydrogenation of diethyl carbonate (DEC) to produce methanol. Furthermore, the catalysts were characterized by physicochemical methods, such as N₂ adsorption, ICP-OES, N₂O titration, SEM, TEM, XRD, H₂-TPR and XPS in detail. Higher copper concentration led to a higher ratio of bulk CuOx species in the calcined samples, which resulted in different copper species distribution after the reduction process. Structure activity relationship analysis indicated that the balance of surface Cu⁰ and Cu⁺ species influenced the formation rate of methanol. A higher proportion of Cu⁺ to (Cu⁺ + Cu⁰) was conducive to methanol formation, while excessive Cu⁰ site density played a negative influence on the methanol synthesized from DEC. Cu/Zn/Al with a 45.2% weight fraction of copper showed better performance with a total methanol formation rate of 131.0 mg g_{cat.}⁻¹ h⁻¹. The reaction temperature and reaction time could obviously affect the reaction performance and the results suggested that 200 °C and 6 h were suitable. Furthermore, the long-term stability and activity of the catalyst was also studied on a fixed bed, and the yield of total methanol reached to 88.5% and the selectivity of total methanol gradually decreased to 74.0% within 200 h, which could be attributed to the detrimental influence derived from the increase of Cu⁰. The reaction pathways involved in the hydrogenation of DEC process were proposed. The substance scope was also extended to other carbonates and the catalyst exhibited superior catalytic performance toward linear carbonates. This work provided insights into carbonate hydrogenation over an effective Cu/Zn/Al catalyst, which could be utilized into upgrading CO₂ indirectly to produce commodity methanol under relatively mild reaction conditions.

 Received 13th January 2020
 Accepted 20th March 2020

DOI: 10.1039/d0ra00347f

rsc.li/rsc-advances

1. Introduction

Chemical utilization of greenhouse gas CO₂ as a feedstock to make value-added chemicals, materials, and transportation fuel

could reduce carbon emission and global warming, as well as providing a long-term solution for the depletion of global reserves of fossil fuels.^{1–4} So far, a series of high value-added chemicals from CO₂ chemical conversion has been achieved, including cyclic carbonates, methanol, formic acid, alkyl carbamates, salicylic acid, dimethyl carbonate (DMC) and so on.^{5,6} Among them, methanol (CH₃OH) is a widely applied bulk chemical and key feedstock for industrial chemicals, which can be further transformed into alternative high molecular weight liquid fuels.⁷ In this regard, hydrogenation of CO₂ into methanol is a promising, efficient, and economical technique for CO₂ utilization.^{8–10} Nevertheless, the reduction/activation of CO₂ into useful liquid products is challenging due to the limitation of thermodynamics and kinetics.^{11,12} Carbonates, which can be produced from CO₂ and alcohols, are reported could be further catalytic hydrogenated to produce methanol under certain circumstances.^{13–16} Thus, carbonates can be deemed as a bridge between CO₂ and methanol to realize indirect hydrogenation of CO₂.^{17–19} As shown in Scheme 1, this route is atom economy and consistent with the green chemistry concept.

^aCAS Key Laboratory of Green Process and Engineering, Institute of Process Engineering, Chinese Academy of Sciences, Beijing, 100190, China. E-mail: lgwang@ipe.ac.cn

^bNational Engineering Laboratory for Hydrometallurgical Cleaner Production Technology, Institute of Process Engineering, Chinese Academy of Sciences, Beijing, 100190, China

^cSino-Danish College, University of Chinese Academy of Sciences, Beijing, 100049, China

^dSino-Danish Center for Education and Research, University of Chinese Academy of Sciences, Beijing, 10049, China

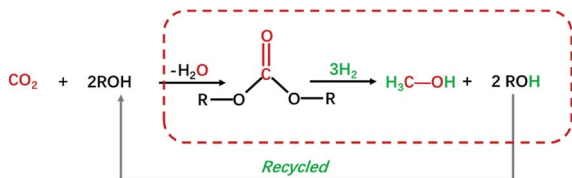
^eSchool of Chemical Engineering, University of Chinese Academy of Sciences, Beijing, 10049, China

^fDalian National Laboratory for Clean Energy, Dalian, 116023, China

^gDepartment of Chemical and Biochemical Engineering, Technical University of Denmark, Lyngby 2800 Kgs, Denmark

† Electronic supplementary information (ESI) available. See DOI: 10.1039/d0ra00347f





Scheme 1 Synthesis of methanol via CO_2 -derived carbonates hydrogenation.

Until now, several groups did researches on this route, and focused on the different catalyst systems. For example, Ding *et al.*²⁰ proposed the route of ethylene carbonate (EC) hydrogenation to co-produce methanol and ethylene glycol, and a homogeneous Ru-based catalyst was applied in this system with nearly full conversion of EC, and selectivity of EG as well as MeOH exceeded 99% at 40 °C. Beller *et al.*²¹ used homogeneous catalyst $\text{Co}(\text{BF}_4)_2$ combined with tridentate phosphine ligands to catalyze carbonates hydrogenation under relatively mild conditions. However, homogeneous catalysts must face the difficulties of separation, reuse, and stability industrially. For heterogeneous catalysts, copper-based catalysts are widely used in selective hydrogenation reactions since they are excellent catalytic active sites for C–O bonds hydrogenation (forming alcohols) and relatively inactive for C–C bond hydrogenolysis (forming low molar weight chemicals like CO_2 , CO and methane).²²

Until now, Cu/HMS, CuCr_2O_4 , Cu/CeO_2 had been reported to catalyze carbonates hydrogenation effectively.^{23–26} Cu/SiO_2 was reported to catalyze dimethyl carbonate (DMC) hydrogenation to methanol, and high copper dispersion and the synergetic effect between balanced Cu^0 and Cu^+ sites contribute to the yield of methanol.²⁶ Dai *et al.*²⁵ applied Cu/CeO_2 nanomaterial in the hydrogenation of diethyl carbonate (DEC) to synthesize methanol, and confirmed the activity of Cu/CeO_2 was influenced by the shape/crystal planes of CeO_2 . Furtherly, they prepared different Cu/CeO_2 nanorod catalysts with various copper concentration and achieved relatively high space-time yield of $8.4 \text{ mmol}_{\text{cat.}}^{-1} \text{ h}^{-1}$, which was due to a high Cu^0 surface area, the moderate ratio of Cu^+/Cu^0 , as well as sufficient surface oxygen vacancies associated with Ce^{3+} .²⁷

In recent years, there has been continued interest in the ternary Cu/Zn/Al catalyst. Industrially, Cu/Zn/Al catalysts have been utilized for methanol synthesis from syngas at typical reaction conditions of 230–280 °C and 5–10 MPa.^{28–30} What's more, Cu/Zn/Al catalyst is a kind of environmentally friendly catalyst with high efficiency in direct CO_2 hydrogenation because of excellent activity for hydrogenation of C=O bond.^{31,32} Hence, the development of effective Cu/Zn/Al catalyst for hydrogenation of carbonate is highly desired both in fundamental research and industrial application.

In this work, ternary Cu/Zn/Al heterogeneous catalysts were prepared by co-precipitation method and were applied in the hydrogenation of DEC into methanol. Moreover, the physico-chemical properties as well as the structures of Cu/Zn/Al catalysts were systematically characterized by various techniques,

including N_2 physisorption, ICP-OES, N_2O titration, XRD, H_2 -TPR, TEM, EDX-mapping, XPS and XAES. Furthermore, the effects of copper concentration, reaction temperature, and reaction time were also investigated. The structure–activity relationship was studied, and the reaction mechanism was proposed. Stability and catalytic performance of catalyst for a long period were also investigated on the fixed bed. At last, Cu/Zn/Al catalyst was also tested on other carbonates.

2. Experimental

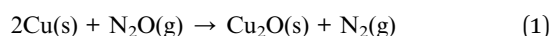
2.1 Catalyst preparation

Typically, ternary Cu/Zn/Al was prepared by co-precipitation method using Na_2CO_3 as a precipitant. In a typical procedure, 1 mol L^{-1} Na_2CO_3 aqueous solution was added to 1 mol L^{-1} mixed metallic aqueous solution of $\text{Cu}(\text{NO}_3)_2 \cdot 3\text{H}_2\text{O}$, $\text{Zn}(\text{NO}_3)_2 \cdot 6\text{H}_2\text{O}$, and $\text{Al}(\text{NO}_3)_3 \cdot 9\text{H}_2\text{O}$ with desired molar ratio of Cu–Zn–Al. Precipitation was carried out with synchronous aging step at 70 °C until pH of the solution achieved to 9, after which the mixture was cooled down to room temperature with stirring. Then, the resulting suspension was recovered by filtration and washed to neutral, then dried at 110 °C overnight and calcined at 500 °C for 5 h in the air. The catalyst was finally obtained by reduction at 500 °C for 3 h in the atmosphere of 10 vol% H_2/N_2 . The Zn/Al ratio was fixed at 1/1 in molar ratio. In this work, a series of Cu/Zn/Al catalysts were prepared with different copper molar ratios of 0.5 : 1 : 1, 1 : 1 : 1, 2 : 1 : 1, 3 : 1 : 1, 4 : 1 : 1, which are denoted as Cu-0.5, Cu-1, Cu-2, Cu-3, Cu-4, respectively. We marked the samples in different preparation stages as Cu/Zn/Al-D (dry precursors), Cu/Zn/Al-C (samples after calcination) and Cu/Zn/Al catalyst (samples after reduction).

2.2 Catalyst characterization

The element contents of catalysts were identified by inductively coupled plasma optical emission spectrometry (ICP-OES) on Agilent ICP-OES730. N_2 physical adsorption measurements were carried using a Quantachrome Autosorb-1 at -196 °C. The BET surface areas were performed *via* the Brunauer–Emmett–Teller (BET) model. The total absorbed pore volumes were received from the nitrogen absorbed volume with a relative pressure of 0.99. Initial estimation of pore size distribution was obtained by Barrett, Joyner and Halenda (BJH) methods based on the isotherm desorption branch. Scanning electron microscopy (SEM) images were measured on a HITACHI SU8020 microscopy. Transmission electron microscopy (TEM), high-resolution transmission electron microscopy (HRTEM) and energy-dispersive X-ray (EDX) images were obtained on field-emission transmission electron microscopy (JEOL, JEM-2100F) using an acceleration voltage of 200 kV. Pre-treatment method was to disperse samples in ethanol ultrasonically for 30 min at ambient temperature. X-ray diffraction (XRD) patterns of samples were recorded in the 2θ range of 10 – 90° on a PANalytical Empyrean diffractometer with $\text{Cu K}\alpha$ radiation ($\lambda = 0.15406 \text{ nm}$). For the X-ray photoelectron spectroscopy (XPS) and X-ray Auger electron spectroscopy (XAES), the powder

catalysts are taken from the sealing bottle. Samples to be tested are then pressed into pieces and glued to the sample stage, after 24 hours in a vacuum, they are performed on a Thermo scalable 250XI system with an Al K α radiation source ($h\nu = 1486.6$ eV) to investigate the surface chemical states of samples. Temperature-programmed reduction (TPR) was performed to give further insight into the reducibility of the catalysts. The H₂-TPR profiles were conducted with a Quantachrome Chembet pulsar TPR/TPD instrument. The TPR profiles were obtained with 5 vol% H₂/Ar flow (40 mL min⁻¹). The temperature was increased from 30 to 750 °C at a rate of 10 °C min⁻¹. The copper dispersity was determined by applying the nitrous oxide chemisorption method and the reactions are described as eqn (1). The catalyst was firstly reduced in a 10 vol% H₂ in argon for 1 h at 450 °C. The samples were cooled at room temperature for 1 hour and then a stream of 10 vol% N₂O/Ar gas was fed into the reactor 40 °C and the effluent gas was analyzed by a thermal conductivity detector (TCD). Nitrogen evolved by the reaction was derived *via* peak area from the TCD signal. A Cu : N₂O = 2 : 1 chemisorption stoichiometry was assumed. S_{Cu} is the surface area of exposed surface copper per gram catalyst, and it was calculated by eqn (2).



$$S_{\text{Cu}} (\text{m}^2\text{g}^{-1}) = \frac{n_{\text{Cu}} N_{\text{A}}}{N_{\text{Cu}} W_{\text{Cat}}} \quad (2)$$

where n_{Cu} is the number of exposed copper atoms, N_{A} is the Avogadro constant equalling to 6.02×10^{23} mol⁻¹, N_{Cu} is the number of copper atoms per square meter (1.4×10^{19}), and W_{Cat} is the weight of catalyst.

2.3 Catalyst performance

The DEC hydrogenation was studied in a 50 mL autoclave. In addition, a fixed-bed reactor was also utilized to investigate the stability and activity of catalysts over a long time. In a typical experiment, 10 mmol DEC and 20 wt% catalyst based on DEC, 10 mL tetrahydrofuran and 20 μL *p*-xylene was added into the reactor. The reactor was then sealed and purged with N₂ five times. After that, 5 MPa H₂ were charged into the reactor at room temperature, and then the reactor was heated to desired temperature and hold for desired time with vigorous mechanical stirring of 600 rpm. After the reaction, the reactor was placed in an icy water bath and the residual gas was released gradually. For the long-period test, 0.5 g catalyst (40–60 mesh) was packed into a stainless-steel tubular reactor (11 mm in inner diameter, 500 mm in length) with a thermocouple inserted into the catalyst bed. And quartz wool was placed on both sides of the catalyst bed. A solution of 10 wt% DEC in tetrahydrofuran (THF) and 2.5 MPa H₂ were fed into the fixed bed at a H₂/DEC molar ratio of 200. The reaction was carried out at 200 °C for 200 h, with the DEC liquid hourly space velocity (LHSV) of 0.2 h⁻¹. After reaction, the used catalysts were dried after rinsing with ethanol and were then kept under seal for further characterizations.

The liquid mixture was analyzed by GC-2014 (Shimadzu Ltd.) equipped with a flame ionization detector (FID), a DB-FFAP

capillary column and an AOC-20i automatic sampler using *p*-xylene (20 μL) as the internal standard. Identification of the liquid products was studied using GCMS (Shimadzu-QP2020). The gas samples were analyzed *via* GC-2014 (Shimadzu Ltd.) equipped with an FID detector and two TCD detectors with seven packed columns. The conversion of DEC, selectivity/yield of detected MeOH were determined by the data from GC-2014 and calculated through the following eqn (3)–(5). In this reaction, a liquid by-product of ethyl methyl carbonate (EMC) was produced through methanol reacting with DEC, and the amount of total methanol produced is the sum of EMC and methanol detected which were calculated through eqn (6)–(9).

$$\text{Conv.}_{\text{DEC}} = \frac{n_{0,\text{DEC}} - n_{\text{DEC}}}{n_{0,\text{DEC}}} \times 100\% = 100\% - \frac{a \times n_{p\text{-xylene}}}{n_{0,\text{DEC}}} \quad (3)$$

$$\text{Sel.}_{\text{MeOH}} = \frac{n_{\text{MeOH}}}{n_{0,\text{DEC}} - n_{\text{DEC}}} \times 100\% = \frac{b \times n_{p\text{-xylene}}}{n_{0,\text{DEC}} - a \times n_{p\text{-xylene}}} \times 100\% \quad (4)$$

$$\text{Yield}_{\text{MeOH}} = \frac{n_{\text{MeOH}}}{n_{0,\text{DEC}}} \times 100\% = \frac{b \times n_{p\text{-xylene}}}{n_{0,\text{DEC}}} \times 100\% \quad (5)$$

$$\text{Sel.}_{\text{EMC}} = \frac{n_{\text{EMC}}}{n_{0,\text{DEC}} - n_{\text{DEC}}} \times 100\% = \frac{c \times n_{p\text{-xylene}}}{n_{0,\text{DEC}} - a \times n_{p\text{-xylene}}} \times 100\% \quad (6)$$

$$\text{Yield}_{\text{EMC}} = \frac{n_{\text{EMC}}}{n_{0,\text{DEC}}} \times 100\% = \frac{c \times n_{p\text{-xylene}}}{n_{0,\text{DEC}}} \times 100\% \quad (7)$$

$$\text{Sel.}_{\text{total}} = \text{Sel.}_{\text{MeOH}} + \text{Sel.}_{\text{EMC}} \quad (8)$$

$$\text{Yield}_{\text{total}} = \text{Yield}_{\text{MeOH}} + \text{Yield}_{\text{EMC}} \quad (9)$$

where, $n_{0,\text{DEC}}$ is the initial mole of DEC, n_{DEC} is the residual mole of DEC, n_{MeOH} is the mole of MeOH detected. n_{EMC} is the mole of EMC. a , b , c are the reaction results calculated and analysed by GC-2014. $n_{p\text{-xylene}}$ is the mole number of *p*-xylene added to the reaction liquid. Furthermore, the activity of catalysts was defined for evaluating the catalytic performance based on the product of methanol and EMC. The physical significance of “Activity” is the formation of methanol per hour by gram catalyst, as a result of this, the unit is $\text{mg g}_{\text{cat.}}^{-1} \text{h}^{-1}$ and the calculation formula is shown in eqn (10) and (11).

$$\text{Methanol formation rate} = \frac{m_{\text{methanol}}}{m_{\text{cat.}} \times t} \quad (10)$$

$$\begin{aligned} \text{Total MeOH formation rate} &= \frac{M_{\text{MeOH}} \times n_{\text{Total}}}{m_{\text{cat.}} \times t} \\ &= \frac{M_{\text{MeOH}} \times (n_{\text{MeOH}} + n_{\text{EMC}})}{m_{\text{cat.}} \times t} \end{aligned} \quad (11)$$

where, $m_{\text{cat.}}$ is the mass weight of the catalyst with the unit of g, M_{MeOH} is the mole weight of methanol and t is the reaction time, h.

Table 1 Texture and catalytic performances of the Cu/Zn/Al catalysts

Entry	Catalyst of Cu/Zn/Al	Atomic ratios of Cu/Zn/Al	N ₂ adsorption/desorption					N ₂ O chemisorption				
			Cu ^a wt%	S _{BET} ^b (m ² g ⁻¹)	V _P ^c (cm ³ g ⁻¹)	d _p ^d (nm)	D ^e (%)	S _{Cu} ^f (m ² g ⁻¹)	DEC conversion ^g and MeOH selectivity ^g (%)	MeOH yield ^g (%)	MeOH formation rate ^g (mg g _{cat.} ⁻¹ h ⁻¹)	
1	Cu-0.5	0.5 : 1 : 1	19.5	74.4	0.32	19.3	9.6	12.7	82.1	43.9	36.0	60.2
2	Cu-1	1 : 1 : 1	35.9	59.2	0.29	21.7	7.0	16.9	83.2	47.1	39.1	63.8
3	Cu-2	2 : 1 : 1	45.2	46.4	0.22	22.8	5.8	17.8	86.1	52.5	45.2	95.6
4	Cu-3	3 : 1 : 1	53.5	41.2	0.18	21.4	5.1	18.4	76.7	46.8	35.9	77.7
5	Cu-4	4 : 1 : 1	72.8	34.6	0.15	20.9	3.8	18.6	66.0	37.5	24.7	41.4

^a Determined by ICP analysis. ^b BET surface area determined by the N₂ adsorption at a relative pressure P/P_0 of 0.99. ^c Total pore volume determined by the N₂ adsorption at a relative pressure P/P_0 of 0.99. ^d Average pore diameter determined by the N₂ adsorption at a relative pressure P/P_0 of 0.99. ^e Cu dispersion degree determined by N₂O titration. ^f Cu surface area determined by N₂O titration. ^g Reaction conditions: 10 mmol DEC, 5 MPa H₂, 10 mL THF, 0.25 g catalyst, 200 °C and 6 h.

3. Results and discussion

3.1 General characterization

Fig. S1† illustrates N₂-physisorption isotherms and the corresponding pore size distributions from the adsorption branches of the catalysts. All curves of Cu-0.5, Cu-1, Cu-2, Cu-3, Cu-4 were of type IV and had mesoporous structure (2 nm < pore diameter < 50 nm).³³ For these samples, the H3 type hysteresis loop (according to IUPAC classification) was observed, which was related to non-rigid aggregates of plate-like particles.^{27,34,35} In addition, with the decreasing of Cu content, the condensation occurred at relatively low pressure. Fig. S1(b)† shows BJH pore size distribution curves from the adsorption branch of the isotherm. Two peaks were observed, of which the first peak showed a broad pore size band in the pore size diameter of 2–10 nm. The second one revealed a relatively low-intensity band in the range of 10–100 nm. Table 1 lists the catalyst composition, textural property and specific copper surface area for each catalyst in this work. BET surface area of Cu/Zn/Al catalysts decreased from 74.4 to 34.6 m² g⁻¹ with copper content rising. Pore volumes of the catalysts were also followed the same trend, which decreased from 0.32 to 0.15 cm³ g⁻¹. What's more, copper dispersion degree of Cu/Zn/Al catalysts were also determined by N₂O titration in Table 1. The dispersion of Cu decreased gradually from 9.6% to 3.8% with the increment of copper concentration from 19.5% (Cu-0.5) to 72.8% (Cu-4).

To study the catalyst structure at different preparation stages, X-ray diffraction patterns was analyzed systematically. The XRD patterns of the five dried precursors Cu-0.5, Cu-1, Cu-2, Cu-3 and

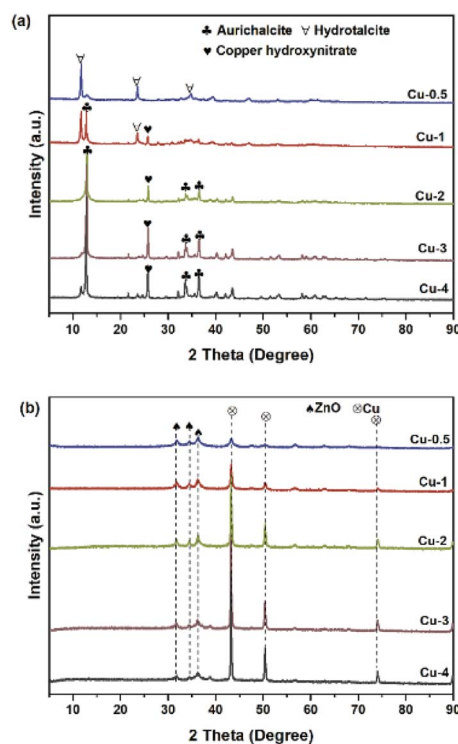


Fig. 1 XRD patterns of (a) Cu/Zn/Al-D; (b) Cu/Zn/Al catalysts (after reduction).

Cu-4 are illustrated in Fig. 1(a). For the curve of Cu-0.5, the sharp peaks of hydrotalcite phase ($\text{Zn}(\text{OH})_2$) at diffraction angles $2\theta = 11.6^\circ$, 23.3° , and 34.5° with good crystallinity were detected, which corresponded to the basal planes (003), (006), and (009), respectively.³⁶ When the copper concentration increased to 45.2% (Cu-2), aurichalcite phase $(\text{Zn,Cu})_5(\text{OH})_6(\text{CO}_3)_2$, were detected at $2\theta = 13.1^\circ$, 34.2° , and 36.7° , which were considered more probability to form interface between copper species and Zn/Al oxide supports.^{37,38} It is worth mentioning that the peak intensity of aurichalcite phase in Cu-2, Cu-3 and Cu-4 increased with copper content increasing, indicating a more intimate contact between copper species and Zn/Al oxide supports with higher copper content. The peak at $2\theta = 25.9^\circ$ is corresponding to the gerhardtite phase of copper hydroxide nitrate ($\text{Cu}_2(\text{OH})_3\text{NO}_3$)³⁹, which further decomposed to CuO in the calcination step.⁴⁰ XRD patterns of calcined samples are shown in Fig. S2(a).† After calcination, the peaks related to hydroxycarbonates in the dry precursors disappeared, but new characteristic peaks of metal oxides were detected. The peaks at $2\theta = 31.8^\circ$, 34.4° , 36.3° , 56.6° and 62.9° are attributed to ZnO with crystalline plane of (1 0 0), (0 0 2), (1 0 1), (1 1 0) and (1 0 3), respectively. The peaks at 35.6° , 38.8° , 48.7° , 58.3° , 61.2° , 65.9° and 68.2° are ascribed to CuO. Crystallization of CuO and ZnO are present in all five samples, while no crystal phases containing aluminum are detected. After calcination, aluminum tends to remain in a mixed oxide phase, which is amorphous state at the relatively lower calcination temperature of 500°C .⁴¹ Fig. 1(b)

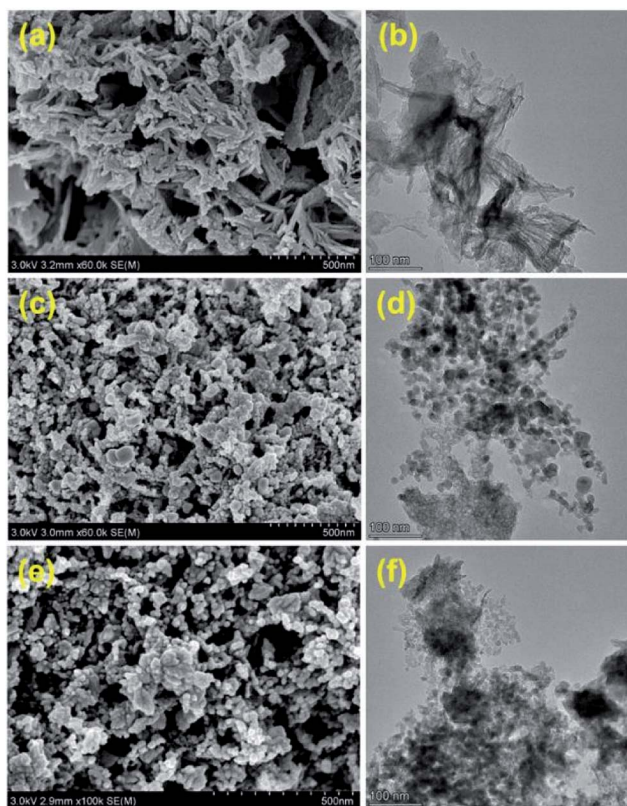


Fig. 2 SEM & HRTEM images of Cu-2 catalyst in different preparation stages, (a) and (b) Cu/Zn/Al-D, (c) and (d) Cu/Zn/Al-C, (e) and (f) Cu-2 catalyst (after reduction).

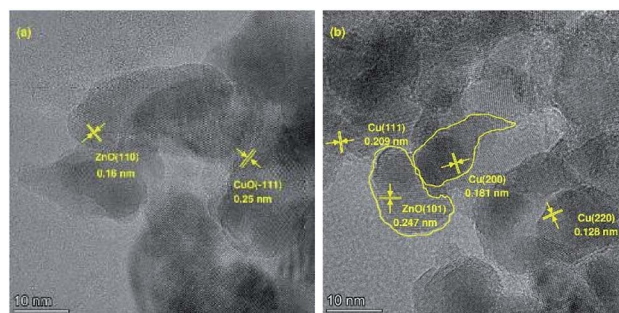


Fig. 3 HRTEM images of samples (a) Cu/Zn/Al-C of Cu-2; (b) Cu-2 catalyst.

shows the XRD patterns of catalysts after reduction with various copper contents. In comparison with XRD patterns before reduction, the samples showed obvious differences. Diffraction peaks of Cu were shown at 43.3° , 50.3° and 73.9° , belonging to the (111), (200), and (220) planes, respectively.^{42,43} When the mass fraction of copper increased, intensities of (111), (200), and (220) diffraction peaks of Cu were enhanced, indicating that the crystallinity of Cu increased. The possible reason is that the reduction of CuO to Cu is an exothermic reaction with $\Delta H = -80.8 \text{ kJ mol}^{-1}$, so copper sintering occurred in the reduction process to a certain degree.⁴⁴

The morphological evolution for different preparation stages of Cu-2 are illustrated in Fig. 2. The sample of dry precursor showed a significant lamellar-like structure (Fig. 2 (a) and (b)). After calcination, morphology of the sample altered from lamellar to spherical. Compared with calcination samples, the morphology of Cu-2 didn't change much after reduction. The surface geometry of the Cu-2 catalyst was further studied by HRTEM (Fig. 3). Before reduction, copper species with a crystal plane of $(-1\ 1\ 1)$ could be observed (Fig. 3(a)), which is in accordance with the results in XRD patterns. In addition, ZnO (1 0 1), Cu^0 (1 1 1), (2 2 0), (2 0 0) can be observed in reduced Cu-2 catalyst after reduction. These results verified that the formation of interface between Cu and Zn/Al oxide, which enable an intimate contact between Cu species and oxide matrix.⁴⁵ EDX elemental mapping in Fig. S3† illustrated that Cu, Zn and Al atoms are all homogeneously dispersed on Cu-2

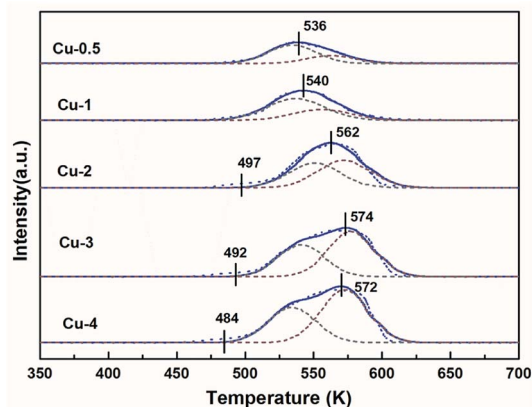


Fig. 4 TPR profiles of Cu/Zn/Al-C with different copper content.

catalyst. TEM images of Cu/Zn/Al catalyst with different copper content in Fig. S4† shows the average particle diameters of Cu/Zn/Al catalysts increased from 7.2 to 8.6 nm with copper content increasing.

H₂-TPR was used to study the reduction behavior of Cu/Zn/Al-C. Fig. 4 shows the TPR profiles of calcined catalysts for different Cu contents, exhibiting a broad reduction peak in the range of 450–600 K. Since ZnO and Al₂O₃ could not be reduced under certain experimental conditions,⁴⁶ these profiles are described to CuO reduction in the CuO/ZnO/Al₂O₃ phase. Generally, the pure CuO was reduced at around 750 K, which was far over these main peaks.⁴⁷ Therefore, it was inferred that the involvement of Zn and Al facilitated the dispersion of copper species and hence reduced the reduction temperature. The reduction of Cu²⁺ to Cu⁺ and Cu⁺ to Cu⁰ are considered as two steps in this reduction process.⁴⁸ To gain more insight into the results of TPR, all profiles were deconvoluted into two Gaussian peaks. According to literatures,^{33,49} the peaks α and β could be ascribed to the reduction of different CuO phases: the low-temperature peak (peak α) was the surface CuO species, which is highly dispersed and influenced by ZnO, the high-temperature peak (peak β) belonged to isolated copper oxide (bulk CuO). Table 3 illustrates that the peak positions and the area proportion of these two peaks. Accordingly, it is seen from Table 3 that the ratio of dispersed CuO decreased with copper concentration increasing, which was in good accordance with trends of Cu dispersion degree determined by N₂O titration in Table 1 and resulting in the difficulty in CuO reduction.

In addition, the onset reduction temperature for Cu-2, Cu-3 and Cu-4 samples decreased gradually, the result of which is in

consistent with XRD curves in Fig. 1(a) that the dry precursors for these three samples showed the enhanced intensities of aurichalcite phase. It is reasonable that more intimate metal contact led to lower onset temperature. The TPR results suggested that higher copper concentration resulted in higher ratio of bulk CuO in the calcined samples, and the percentage of dispersed CuO and bulk CuO might influence the reduction process, as well as the ratio of Cu⁺/(Cu⁺ + Cu⁰).

XPS-XAES was measured to confirm the chemical states of samples. The results were shown in Fig. 5 and 6, and the relevant quantitative data were summarized in Table 2. For all calcined samples, the XPS peaks at around 933.4 eV binding energy corresponding to Cu 2p_{3/2} and the shake-up of satellite peaks indicated that copper state was +2, which was consistent with XRD results. After the reduction process, the photoelectron peak of Cu 2p_{3/2} at about 932.6 eV towards lower binding energy and the absence of the satellite peaks suggested that Cu²⁺ species had been reduced to metallic Cu⁰ and/or Cu⁺. To better distinguish Cu⁰ and Cu⁺, the X-ray induced Auger spectrum of Cu LMM was also investigated. The peak positions, as well as the values of Cu⁺% derived from the deconvolution were summarized in Table 2. The asymmetric and broad peaks of Cu/Zn/Al catalysts were deconvoluted into two overlapping Cu LMM Auger kinetic energy peaks at around 917.0 eV and 918.8 eV, representing Cu⁺ and Cu⁰, respectively.

Although the *ex situ* re-oxidation of Cu and Cu₂O in air could not be excluded completely, it usually required high temperature in oxygen atmosphere for effective oxidation of Cu⁰ to Cu⁺.^{50–52} In this work, as also verified by XPS results, there are not detectable CuO species in Cu/Zn/Al catalysts because of the absence of the characteristic satellite peaks. Therefore, the state of copper kept stable essentially during the characterization. As shown in Table 2, the ratio of Cu⁺/(Cu⁺ + Cu⁰) first rose and then decreased with the

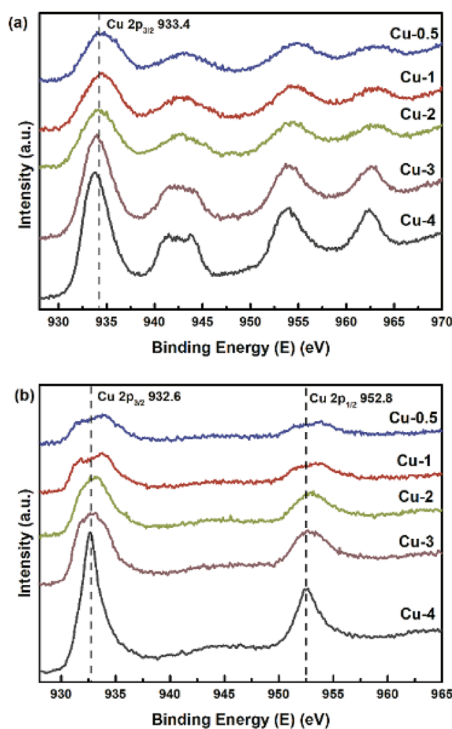


Fig. 5 Cu 2p XP spectra of Cu/Zn/Al-C (a), and Cu/Zn/Al catalysts (b).

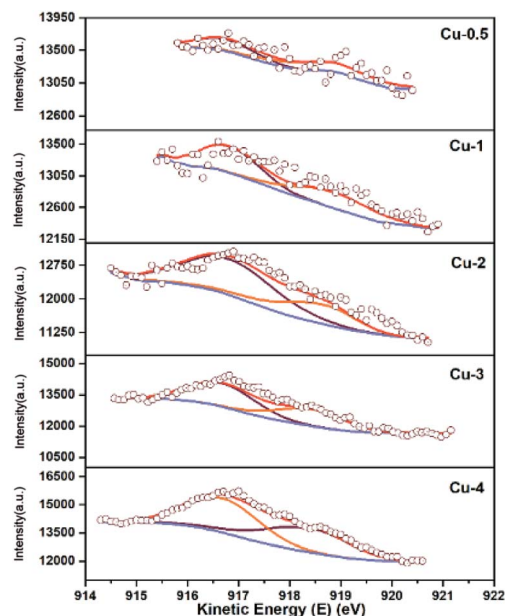


Fig. 6 Cu LMM XAES spectra of Cu/Zn/Al catalysts with different copper contents.

Table 2 H₂-TPR data of all prepared Cu/Zn/Al-C

Entry	Catalyst	TPR peak position (temperature/K) and area proportion (%)			
		Peak α		Peak β	
1	Cu-0.5	533.8 K	69.9%	562.3 K	30.1%
2	Cu-1	539.4 K	66.9%	565.2 K	33.1%
3	Cu-2	548.9 K	47.0%	570.5 K	53.0%
4	Cu-3	539.4 K	41.3%	576.2 K	58.7%
5	Cu-4	534.2 K	40.0%	572.7 K	60.0%

increase of copper concentration. The binding energy values of Zn ($2p_{1/2}$) and Zn ($2p_{3/2}$) were around 1046 eV and 1023 eV, respectively, which were closed to the energy peaks (1044.8 eV and 1021.8 eV) of ZnO.⁵³ Moreover, there was an energy difference of 23 eV between Zn ($2p_{1/2}$) and Zn ($2p_{3/2}$) peaks, which is equivalent to that of ZnO.⁵⁴ In addition, the spectrum recorded Al 2p peaks with the binding energy from 74.1–74.4 eV,^{55,56} which are characteristic for Al³⁺ ions in Al₂O₃. The XPS results showed a good agreement with the corresponding XRD analysis.

3.2 Catalytic performance of Cu/Zn/Al catalysts

The catalytic performance of Cu/Zn/Al catalysts with different Cu concentration for the hydrogenation of DEC was performed under 200 °C for 6 h, and the results were summarized in Table 1. Increase in the copper concentration led to an increase firstly and then decrease in DEC conversion. The selectivity of methanol and methanol formation rate reached to the maximum on the Cu-2 catalyst (45.2%). For all the Cu/Zn/Al catalysts, methanol and ethanol were the main liquid products with the small amount of ethyl methyl carbonate (EMC). EMC is a by-product in heterogeneously catalyzed DEC hydrogenation probably resulting from transesterification of produced methanol and unreacted DEC. This transesterification was verified over Cu/Zn/Al catalyst (Cu-2) at 200 °C as well as on Zn/Al catalyst in Scheme S1,[†] which indicated that Zn/Al could facilitate the transesterification of methanol and DEC. For the gas products, CO₂ and CO could be detected (Fig. S6[†]). The majority of gas products was CO₂ which was considered to be produced through hydrolysis reaction between DEC and a small amount of water contained in the solvent,⁵⁷ which could further react with H₂ to form CO.²⁶ Notably, the methanol formation rate reached to the

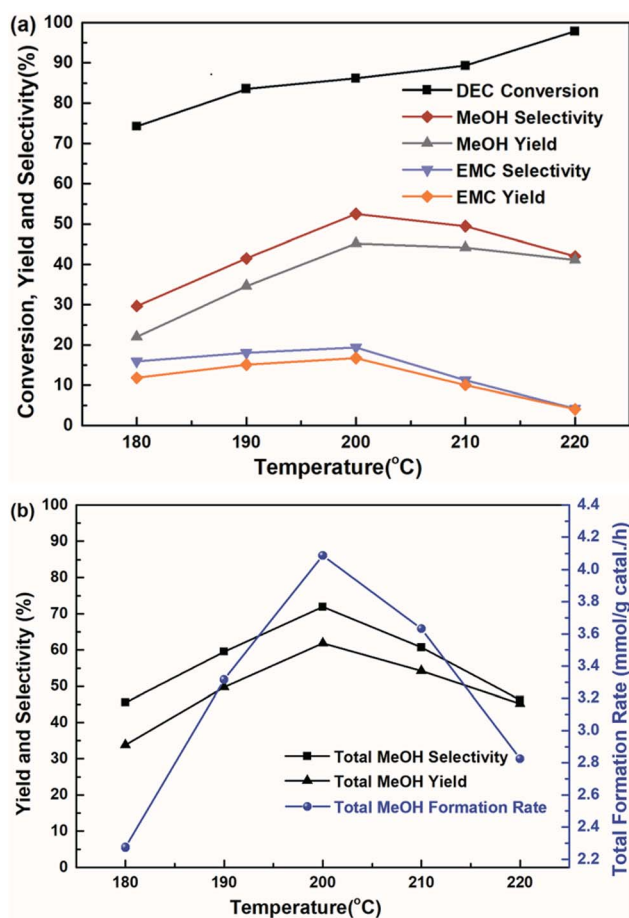


Fig. 7 The effect of reaction temperature on the hydrogenation of DEC for 6 h, (a) methanol, EMC, and DEC, (b) total methanol, based on the dosage of 10 mmol DEC, 5 MPa H₂, 10 mL THF and 0.24 g Cu-2 catalyst (20 wt% DEC).

maximum of 95.6 mg g_{cat.}⁻¹ h⁻¹ at the highest Cu⁺/(Cu⁺ + Cu⁰) ratio of 0.69 among the catalysts tested. The percentage of Cu⁺ increased in the order of Cu-4 < Cu-0.5 < Cu-1 < Cu-3 < Cu-2 as shown in Table 2, the order of which is the same as the methanol formation rate and methanol selectivity. Hence, it could conceivably be hypothesised that the catalytic activity is highly related to the ratio of Cu⁺/(Cu⁺ + Cu⁰).

The influence of reaction temperature on the catalytic activity was carried out in the range of 180–220 °C at 6 h, shown

Table 3 XPS-XAES data of Cu/Zn/Al catalysts

Entry	Catalysts	Cu wt%	Binding energy (eV)				Binding energy (eV)		Cu ⁺ /(Cu ⁺ + Cu ⁰) (molar ratio)
			Cu 2p _{3/2}	Zn 2p _{1/2}	Zn 2p _{3/2}	Al 2p	Cu ⁺	Cu ⁰	
1	Cu-0.5	19.5	933.4	1046.1	1023.2	74.1	917.3	919.3	0.45
2	Cu-1	35.9	933.3	1046.4	1023.2	74.2	916.9	918.8	0.56
3	Cu-2	45.2	932.9	1046.0	1022.9	74.4	916.8	918.7	0.69
4	Cu-3	53.5	932.7	1046.1	1023.1	74.4	916.8	918.7	0.57
5	Cu-4	72.8	932.6	1045.5	1022.6	73.4	916.9	918.7	0.45

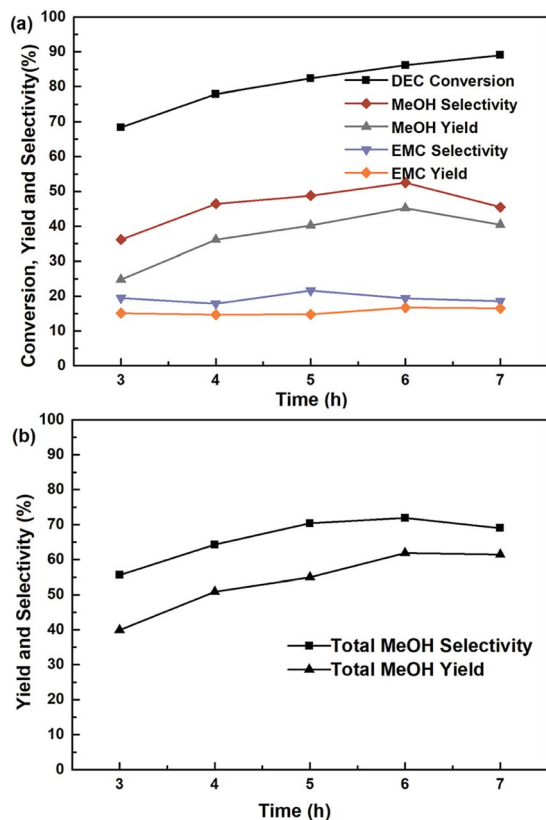


Fig. 8 The effect of reaction time at 200 °C on the hydrogenation of DEC, (a) methanol, EMC and DEC, (b) total methanol, based on the dosage of 10 mmol DEC, 5 MPa H₂, 10 mL THF and 0.24 g Cu-2 catalyst (20 wt% DEC).

in Fig. 7. It is found that the reaction temperature had a significant effect on the performance of the catalyst, and the higher of the reaction temperature, the more favourable of the DEC conversion. The DEC conversion could reach to the highest of 97.8% when the temperature increased to 220 °C. However, selectivity and yield of methanol and EMC firstly increased and

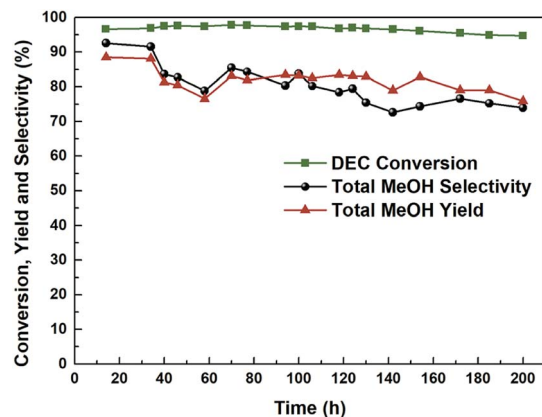


Fig. 9 Hydrogenation performance of Cu-2 catalyst as a function of time on stream. Temperature: 200 °C, liquid hour space velocity (LHSV) $\sim 0.2 \text{ h}^{-1}$, H₂/DEC = 200, 2.5 MPa.

then decreased, accompanied by elevating reaction temperature. Noteworthy to say, since part of the methanol was further transesterified with DEC to produce by-product EMC, the total methanol yield was defined as the summary of detected methanol and EMC produced from methanol. And the trends of total methanol yield/selectivity/formation rate in Fig. 7(b) showed the same trends with the selectivity/yield of methanol and EMC in Fig. 7(a). All of them showed the highest data at the temperature of 200 °C, because the reaction temperature exceeding 200 °C might promote DEC hydrolysis, which caused a decrease of yield and selectivity of methanol, as well as total methanol. The effect of reaction time on the catalytic performance was also investigated and the results was shown in Fig. 8, the conversion of DEC increased gradually from 68.4% to 89.0% with reaction time increasing from 3 to 7 h. The selectivity and yield of methanol increased to 52.5% and 45.2% at 6 h but declined slightly when the reaction time further prolonged to 7 h. The total methanol selectivity and yield also increased gradually to maximum values at 6 h, 71.9% and 61.9%, respectively. The results in Fig. 7 and 8 implied that 200 °C and 6 h is an optimized temperature and a favourable reaction time, respectively.

3.3 Stability of Cu/Zn/Al catalyst

It is crucial for industrial application to study the long-term stability and activity of the catalyst. Fig. 9 and S5† plots the catalytic activity as a function of reaction time for the most efficient Cu-2 catalyst for DEC hydrogenation. It is obviously seen that DEC conversion stayed at around 95.0% over a 200 h reaction time, while the total methanol yield/selectivity was over

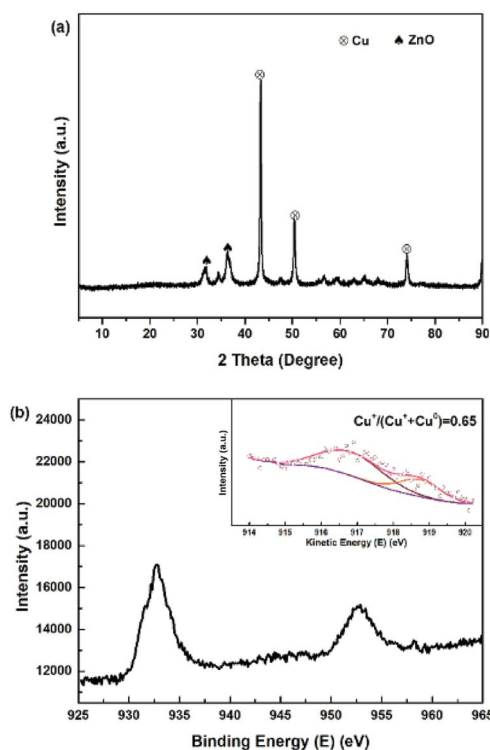
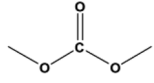
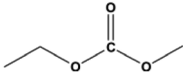
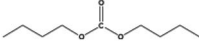
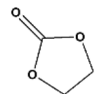
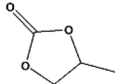


Fig. 10 (a) XRD and (b) XPS-XAES of used Cu-2 catalyst after running 200 h.

Table 4 The scope of carbonates for methanol synthesis^a

Entry	Substrate	Time (h)	Conversion (%)	MeOH selectivity (%)	MeOH yield (%)
1		8	100	76.8	76.8
2		8	98.9	49.1	48.6
3		8	99.4	41.2	38.9
4		8	82.7	15.2	12.6
5		6	98.7	7.0	6.9

^a Reaction conditions: the hydrogenation of carbonates are achieved at 200 °C, the dosage of carbonates is 10 mmol, in the solvent of 10 mL THF and 20 wt% Cu-2 catalyst (based on the carbonates).

80.0% before the first 40 h, which showed good performance.²⁷ However, both methanol and total methanol selectivity/yield declined slightly within 200 h. The decline of selectivity/yield might be explained by the fact that part of Cu⁺ was reduced by the H₂ during the hydrogenation process, leading to the decrease of Cu⁺/(Cu⁺ + Cu⁰) ratio. This result was further verified by comparing Cu LMM XAES spectra of Cu-2 catalyst before and after 200 h of reaction (Fig. 10) that, the ratio of Cu⁺/(Cu⁺ + Cu⁰) decreased from 0.69 to 0.65.

3.4 Performance of Cu-2 on different scope of the carbonates

The applicability for a variety of symmetrical and/or asymmetrical carbonates, *e.g.*, DMC, ethyl methyl carbonate, EMC, dibutyl carbonate (DBC), ethylene carbonate (EC), propylene carbonate (PC) over Cu-2 catalyst was surveyed at 200 °C and 5 MPa H₂ initial pressure. Table 4 provides the summary statistics for the corresponding results.

For the hydrogenation of DMC, 76.8% yield of methanol could be obtained with 100% DMC conversion within 8 h, entry 1. For the hydrogenation of other carbonates linear, EMC and DBC, 48.6% and 38.9% methanol yield were obtained, respectively, and both of the conversion exceeded 98.9%. However, Cu-2 did not perform well on cyclic carbonates, *i.e.* EC and PC (entries 4 and 5), which was possibly caused by decomposition of cyclic carbonates in the presence of Zn/AlO_x.⁵⁸

3.5 Mechanism of the hydrogenation of DEC over Cu/Zn/Al catalysts

Above all, it is considered that Cu in the Cu/Zn/Al catalyst played a vital role in methanol synthesis from DEC hydrogenation. Without Cu, the binary catalyst Zn/Al can't promote the production of methanol from DEC and H₂ (Scheme S1†). What's

more, the synergistic cooperation of Cu⁰ and Cu⁺ sites, formed through CuO reduction, played a key role for the high performance of Cu/Zn/Al catalysts in the hydrogenation process.

Fig. 11 shows the ratio of Cu⁺/(Cu⁺ + Cu⁰) and specific surface area S_{Cu} as a function of copper concentration. It could be found that the Cu⁺/(Cu⁺ + Cu⁰) showed a volcanic trend as a function of Cu concentration. The formation of stabilized Cu⁺ is considered to be related to the interface between copper species and metal oxide support, while the formation of Cu⁰ is considered to be originated from the bulk CuO.⁵⁹⁻⁶¹ At the beginning of copper loading increase, Cu⁺/(Cu⁺ + Cu⁰) values initially increased because of the increase of relative interface area between Cu and Zn/Al species, thus resulting in the formation of more Cu⁺-O-Zn/Al like structures at the interface.⁶² After the copper concentration reached to a certain

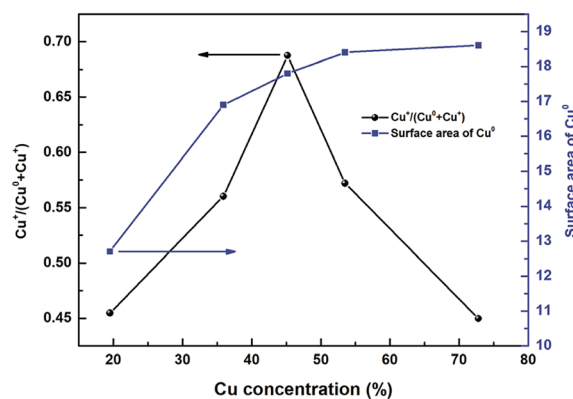


Fig. 11 S_{Cu} (m² g_{cat.}⁻¹) and Cu⁺/(Cu⁺ + Cu⁰) as a function of Cu concentration.

degree, the ratio of bulk CuO continued to increase (Table 2 peak β area proportion) but the relative interface area between copper species and Zn/Al oxides decreased. Therefore, the proportion of Cu^+ decreased from 0.69 to 0.45. As a result, the ratio of $\text{Cu}^+ / (\text{Cu}^+ + \text{Cu}^0)$ showed a volcanic trend as a function of Cu concentration. The conclusion had been come up with in catalytic performance part that the catalytic activity is highly related to the ratio of Cu^+ sites. Higher $\text{Cu}^+ / (\text{Cu}^+ + \text{Cu}^0)$ ratio led to higher methanol formation rate. While, the correlation in Fig. 11 demonstrates the optimal methanol formation rate on the Cu/Zn/Al catalysts lies not only in Cu^+ , but also in Cu^0 . However, excessive Cu^0 sites density would play a negative influence on the methanol synthesis, which meant a balanced distribution of surface Cu^0 and Cu^+ species is considered to be an essential factor to obtain outstanding performance in the hydrogenation of carbonates.

Studies showed that Cu^+ played as a function of adsorbing and stabilizing the intermediate products in the reaction and acts as an electrophilic or Lewis acid site to polarize the $\text{C}=\text{O}$ bond through an electron lone pair on the oxygen, thereby increasing the reactivity of the ester group.^{63,64} While Cu^0 species played as a function of absorption and activation of H_2 *via* splitting hydrogen, which provided H atoms for reactant/intermediates.⁶⁵ It should be noted that, excessive Cu^0 sites lead to more H_2 splitting, which will be transferred *via* spillover from metallic Cu particles to ZnO surface.⁵⁷ This meant the function of ZnO, acting as electronic promoter to absorb ester groups,^{32,62} were suppressed. Thus, the excessive hydrogen spillover between Cu and ZnO led to the insufficient absorption coverage of the carbonates or reaction intermediate, leading the conversion of DEC decreased. Also, HRTEM results had verified the formation of interface between Cu and Zn/Al oxide in this paper, which is contribute to the high dispersion of Cu. In addition, Al_2O_3 was observed in XPS result and was considered as promoter to enhance the long-term stability, besides, the addition of Al has been reported to enhance the BET surface area and Cu dispersion as well as restrain copper particles sintering.⁶² In this paper, we think Al_2O_3 mainly played a supporting role and worked as a structure promoter.⁵⁷

Based on our experimental results and analysis, a possible mechanism was proposed for DEC hydrogenation into

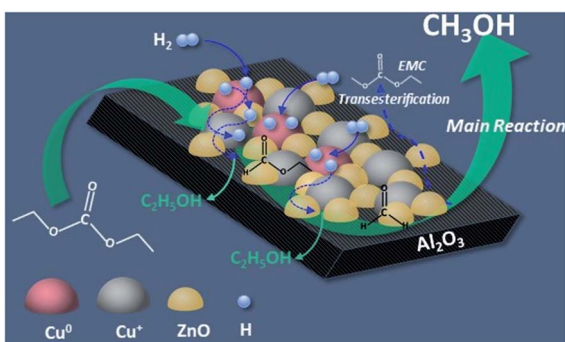


Fig. 12 The possible mechanism of DEC hydrogenation to produce methanol.

methanol over Cu/Zn/Al, and the process is shown in Fig. 12. The whole process includes three steps, firstly, Cu^+ species and ZnO adsorbs the ester groups of DEC. At the same time, H_2 is absorbed and splitted into H atoms on Cu^0 species. H atoms, which are then transferred to ZnO surface and trapped at the surface, further migrate to other Cu particles, and react with the absorbed DEC to form ethyl formate with one molecular of ethanol released at the surface of the catalyst (step 1); then, the formed ethyl formate continued react with H atoms to form formaldehyde with another molecular of ethanol released (step 2); at last, formaldehyde was hydrogenated by H atoms into methanol (step 3). Meanwhile, Zn/Al binary catalyst promoted the formation of EMC through transesterification reaction of methanol and DEC.

4. Conclusions

In this work, a series of Cu/Zn/Al catalysts with various copper concentrations were prepared by the co-precipitation method with synchronous aging step, which were applied in DEC hydrogenation. All catalysts possessed disordered mesoporous structures. In the preparation process, the morphology of samples altered from lamellar to spherical. Copper species of Cu^+ and Cu^0 were considered as active sites, and they had synergistic effect on the hydrogenation of DEC. The highest $\text{Cu}^+ / (\text{Cu}^+ + \text{Cu}^0)$ value led to the best performance of catalyst (Cu-2). However, excessive Cu^0 sites resulted in the decline of DEC conversion, since hydrogen spillover between Cu and ZnO influenced the absorption of carbonates/intermediate. Aluminum functioned as a support in the form of Al_2O_3 . ZnO played the role of physical spacer between copper species and helped dispersing the Cu phase during the catalyst preparation, thus brought more intimate interface contact between Cu and Zn/Al oxide.

At the optimized temperature of 200 °C and time of 4 h, Cu-2 catalyst with 45.2% mass fraction exhibited 86.1% DEC conversion and 71.9% total methanol selectivity with 131.0 mg $\text{g}_{\text{cat}}^{-1} \text{h}^{-1}$ total methanol formation rate under 5 MPa. Time-on-stream experiments on a fixed bed showed that the conversion of DEC kept around 95.0% with a small declining selectivity of methanol over a 200 h reaction time at 200 °C and 2.5 MPa H_2 , and thus Cu-2 catalyst provided a long-term stability. This work provided a facile Cu/Zn/Al catalyst, which could be utilized into indirectly upgrading CO_2 to produce commodity methanol under relatively mild reaction conditions.

Conflicts of interest

There are no conflicts to declare.

Acknowledgements

The authors acknowledge the National Natural Science Foundation of China (21576272), "Transformational Technologies for Clean Energy and Demonstration", Strategic Priority Research Program of the Chinese Academy of Sciences, Grant No. XDA 21030600. We also acknowledge the project from

Science and Technology Service Network Initiative, Chinese Academy of Sciences (KFJ-STIS-QYZD-138) for financial supports.

Notes and references

- 1 A. K. Ahmed Al-Mamoori, A. A. Rownaghi and F. Rezaei, *Energy Technol.*, 2017, **5**, 834–849.
- 2 I. Dimitriou, P. García-Gutiérrez, R. H. Elder, R. M. Cuéllar-Franca, A. Azapagic and R. W. K. Allen, *Energy Environ. Sci.*, 2015, **8**, 1775–1789.
- 3 M. He, Y. Sun and B. Han, *Angew. Chem., Int. Ed. Engl.*, 2013, **52**, 9620–9633.
- 4 L. Wang, L. Wang, J. Zhang, X. Liu, H. Wang, W. Zhang, Q. Yang, J. Ma, X. Dong, S. J. Yoo, J. G. Kim, X. Meng and F. S. Xiao, *Angew. Chem., Int. Ed. Engl.*, 2018, **57**, 6104–6108.
- 5 E. A. Quadrelli, G. Centi, J. L. Duplan and S. Perathoner, *ChemSusChem*, 2011, **4**, 1194–1215.
- 6 S. N. Riduan and Y. Zhang, *Dalton Trans.*, 2010, **39**, 3347–3357.
- 7 I. Yarulina, A. D. Chowdhury, F. Meirer, B. M. Weckhuysen and J. Gascon, *Nat. Catal.*, 2018, **1**, 398–411.
- 8 K. Larmier, W.-C. Liao, S. Tada, E. Lam, R. Verel, A. Bansode, A. Urakawa, A. Comas-Vives and C. Coperet, *Angew. Chem., Int. Ed.*, 2017, **56**, 2318–2323.
- 9 E. S. Van-Dal and C. Bouallou, *J. Cleaner Prod.*, 2013, **57**, 38–45.
- 10 S. Kar, R. Sen, A. Goepfert and G. K. S. Prakash, *J. Am. Chem. Soc.*, 2018, **140**, 1580–1583.
- 11 R. M. Cuéllar-Franca and A. Azapagic, *J. CO₂ Util.*, 2015, **9**, 82–102.
- 12 J. L. Wang, C. X. Miao, X. Y. Dou, J. Gao and L. N. He, *Curr. Org. Chem.*, 2011, **15**, 621–646.
- 13 L. G. Wang, H. Q. Li, S. M. Xin, P. He, Y. Cao, F. J. Li and X. J. Hou, *Appl. Catal., A*, 2014, **471**, 19–27.
- 14 X. Zhang, D. Jia, J. Zhang and Y. Sun, *Catal. Lett.*, 2014, **144**, 2144–2150.
- 15 F. Gasc, S. Thiebaud-Roux and Z. Mouloungui, *J. Supercrit. Fluids*, 2009, **50**, 46–53.
- 16 O. Arbelaez, A. Orrego, F. Bustamante and A. Luz Villa, *Top. Catal.*, 2012, **55**, 668–672.
- 17 E. Balaraman, C. Gunanathan, J. Zhang, L. J. Shimon and D. Milstein, *Nat. Chem.*, 2011, **3**, 609–614.
- 18 X. L. Du, Z. Jiang, D. S. Su and J. Q. Wang, *ChemSusChem*, 2016, **9**, 322–332.
- 19 M. Cui, Q. Qian, Z. He, Z. Zhang, J. Ma, T. Wu, G. Yang and B. Han, *Chem. Sci.*, 2016, **7**, 5200–5205.
- 20 Z. B. Han, L. C. Rong, J. Wu, L. Zhang, Z. Wang and K. L. Ding, *Angew. Chem., Int. Ed.*, 2012, **51**, 13041–13045.
- 21 F. Ferretti, F. K. Scharnagl, A. Dall'Anese, R. Jackstell, S. Dastgir and M. Beller, *Catal. Sci. Technol.*, 2019, **9**, 3548–3553.
- 22 Y. Wang, Y. Shen, Y. Zhao, J. Lv, S. Wang and X. Ma, *ACS Catal.*, 2015, **5**, 6200–6208.
- 23 X. Chen, Y. Cui, C. Wen, B. Wang and W.-L. Dai, *Chem. Commun.*, 2015, **51**, 13776–13778.
- 24 C. Lian, F. Ren, Y. Liu, G. Zhao, Y. Ji, H. Rong, W. Jia, L. Ma, H. Lu, D. Wang and Y. Li, *Chem. Commun.*, 2015, **51**, 1252–1254.
- 25 Y. Cui and W.-L. Dai, *Catal. Sci. Technol.*, 2016, **6**, 7752–7762.
- 26 Y. Cui, X. Chen and W.-L. Dai, *RSC Adv.*, 2016, **6**, 69530–69539.
- 27 H. Li, Y. Cui, Q. Liu and W.-L. Dai, *ChemCatChem*, 2018, **10**, 619–624.
- 28 T. S. Askgaard, J. K. Norskov, C. V. Ovesen and P. Stoltze, *J. Catal.*, 1995, **156**, 229–242.
- 29 G. Busca, U. Costantino, F. Marmottini, T. Montanari, P. Patrono, F. Pinzari and G. Ramis, *Appl. Catal., A*, 2006, **310**, 70–78.
- 30 R. Q. Yang, X. C. Yu, Y. Zhang, W. Z. Li and N. Tsubaki, *Fuel*, 2008, **87**, 443–450.
- 31 L. M. He, H. Y. Cheng, G. F. Liang, Y. C. Yu and F. Y. Zhao, *Appl. Catal., A*, 2013, **452**, 88–93.
- 32 Q. Hu, G. L. Fan, S. Y. Zhang, L. Yang and F. Li, *J. Mol. Catal. A: Chem.*, 2015, **397**, 134–141.
- 33 M. Bahmani, B. V. Farahani and S. Sahebdelfar, *Appl. Catal., A*, 2016, **520**, 178–187.
- 34 K. Kaneko, *J. Membr. Sci.*, 1994, **96**, 59–89.
- 35 M. M. Yusoff, N. Yahaya, N. M. Saleh and M. Raoov, *RSC Adv.*, 2018, **8**, 25617–25635.
- 36 D. Hammoud, C. Gennequin, A. Aboukais and E. A. Aad, *Int. J. Hydrogen Energy*, 2015, **40**, 1283–1297.
- 37 C. Baltes, S. Vukojevic and F. Schueth, *J. Catal.*, 2008, **258**, 334–344.
- 38 I. Atake, K. Nishida, D. Li, T. Shishido, Y. Oumi, T. Sano and K. Takehira, *J. Mol. Catal. A: Chem.*, 2007, **275**, 130–138.
- 39 D. C. Pereira, D. L. A. de Faria and V. R. L. Constantino, *J. Braz. Chem. Soc.*, 2006, **17**, 1651–1657.
- 40 N. Guillou, M. Louer and D. Louer, *J. Solid State Chem.*, 1994, **109**, 307–314.
- 41 S. Y. Cheng, J. W. Kou, Z. H. Gao and W. Huang, *Appl. Catal., A*, 2018, **556**, 113–120.
- 42 M. Salavati-Niasari and F. Davar, *Mater. Lett.*, 2009, **63**, 441–443.
- 43 C. L. Huang, J. J. Wen, Y. H. Sun, M. Y. Zhang, Y. F. Bao, Y. D. Zhang, L. Liang, M. L. Fu, J. L. Wu, D. Q. Ye and L. M. Chen, *Chem. Eng. J.*, 2019, **374**, 221–230.
- 44 C. Rhodes, G. J. Hutchings and A. M. Ward, *Catal. Today*, 1995, **23**, 43–58.
- 45 J. Anton, J. Nebel, H. Q. Song, C. Froese, P. Weide, H. Ruland, M. Muhler and S. Kaluza, *Appl. Catal., A*, 2015, **505**, 326–333.
- 46 I. Melian-Cabrera, M. L. Granados and J. L. G. Fierro, *J. Catal.*, 2002, **210**, 273–284.
- 47 K. W. Jun, W. J. Shen, K. S. R. Rao and K. W. Lee, *Appl. Catal., A*, 1998, **174**, 231–238.
- 48 S. Kuhl, A. Tarasov, S. Zander, I. Kasatkin and M. Behrens, *Chem.–Eur. J.*, 2014, **20**, 3782–3792.
- 49 F. Zhang, Y. Liu, X. Y. Xu, P. P. Yang, P. Miao, Y. L. Zhang and Q. Sun, *Fuel Process. Technol.*, 2018, **178**, 148–155.
- 50 J. Y. Zheng, T.-K. Van, A. U. Pawar, C. W. Kim and Y. S. Kang, *RSC Adv.*, 2014, **4**, 18616.

- 51 M. A. Badillo-Avila, R. Castanedo-Perez, J. Marquez-Marin, D. E. Guzman-Caballero and G. Torres-Delgado, *Mater. Chem. Phys.*, 2019, **236**, 13.
- 52 J. Gong, H. Yue, Y. Zhao, S. Zhao, L. Zhao, J. Lv, S. Wang and X. Ma, *J. Am. Chem. Soc.*, 2012, **134**, 13922–13925.
- 53 H. Abdullah and D. H. Kuo, *ACS Appl. Mater. Interfaces*, 2015, **7**, 26941–26951.
- 54 Y. Chen, H. Ding and S. Sun, *Nanomaterials*, 2017, **7**, 217.
- 55 A. Hess, E. Kemnitz, A. Lippitz, W. E. S. Unger and D. H. Menz, *J. Catal.*, 1994, **148**, 270–280.
- 56 G. Lietz, K. H. Schnabel, C. Peuker, T. Gross, W. Storek and J. Volter, *J. Catal.*, 1994, **148**, 562–568.
- 57 K. Shukla and V. C. Srivastava, *RSC Adv.*, 2016, **6**, 32624–32645.
- 58 S. Searles, D. G. Hummel, S. Nukina and P. E. Throckmorton, *J. Am. Chem. Soc.*, 1960, **82**, 2928–2931.
- 59 Y. Okamoto, K. Fukino, T. Imanaka and S. Teranishi, *Chem. Lett.*, 1984, **1**, 71–74.
- 60 J. Y. Kim, J. A. Rodriguez, J. C. Hanson, A. I. Frenkel and P. L. Lee, *J. Am. Chem. Soc.*, 2003, **125**, 10684–10692.
- 61 Y. Zhao, H. Zhang, Y. Xu, S. Wang, Y. Xu, S. Wang and X. Ma, *J. Energy Chem.*, 2020, **49**, 248–256.
- 62 W. Li, G. Fan, L. Yang and F. Li, *Catal. Sci. Technol.*, 2016, **6**, 2337–2348.
- 63 H. Liu, Z. Huang, Z. Han, K. Ding, H. Liu, C. Xia and J. Chen, *Green Chem.*, 2015, **17**, 4281–4290.
- 64 T. Fujitani and J. Nakamura, *Catal. Lett.*, 1998, **56**, 119–124.
- 65 Y. Y. Cui, X. Chen and W. L. Dai, *RSC Adv.*, 2016, **6**, 69530–69539.